NASA

Technical Memorandum 80729

LAPR: AN EXPERIMENTAL AIRCRAFT PUSHBROOM SCANNER

S. W. WHARTON, J. R. IRONS AND F. HUEGEL

(NASA-TM-80729) LAPR: AN EXPERIMENTAL AIRCRAFT PUSHBROOM SCANNER (National Aeronautics and Space Administration) 31 p
HC A03/MF A01 CSCL 14B G3/43

N81-20493
Unclas
31319

JULY 1980

National Aeronautics and Space Administration

Goddard Space Flight Center
Greenbelt, Maryland 20771

TM 80729

LAPR: AN EXPERIMENTAL AIRCRAFT PUSHBROOM SCANNER*

S. W. Wharton and J. R. Irons
Earth Resources Branch - Code 923
F. Huegel
Experiment Engineering Branch - Code 944

July 1980

*This is a preprint of a manuscript submitted to Photogrammetric Engineering and Remote Sensing.

GODDARD SPACE FLIGHT CENTER
Greenbelt, Maryland

LAPR: AN EXPERIMENTAL AIRCRAFT PUSHBROOM SCANNER

S. W. Wharton and J. R. Irons
Earth Resources Branch - Code 923

F. Huegel
Experiment Engineering Branch - Code 944

ABSTRACT

A three band Linear Array Pushbroom Radiometer (LAPR) was built and flown on an experimental basis by NASA, at the Goddard Space Flight Center. The functional characteristics of the instrument and the methods used to preprocess the data, including radiometric correction, are described. The radiometric sensitivity of the instrument was tested and compared to that of the Thematic Mapper and the Multispectral Scanner. The radiometric correction procedure was evaluated quantitatively, using laboratory testing; and qualitatively, via visual examination of the LAPR test flight imagery.

Although effective radiometric correction could not yet be demonstrated via laboratory testing, radiometric distortion did not preclude the visual interpretation or parallelpiped classification of the test imagery.

CONTENTS

LIST OF TABLES

LIST OF TABLES (Continued)

LIST OF FIGURES

LAPR: AN EXPERIMENTAL AIRCRAFT PUSHBROOM SCANNER

I. INTRODUCTION

A three band Linear Array Pushbroom Radiometer (LAPR) was designed and built as an engineering research instrument for experimental use on aircraft by the Earth Observations Systems Division at the NASA Goddard Space Flight Center (GSFC). The LAPR is currently undergoing extensive calibration, evaluation, and testing, as part of an engineering program to explore the applications of multispectral linear array (MLA) technology to space flight instruments. This program involves both laboratory and flight testing. Flights are coordinated with personnel within the Earth Resources Branch at NASA/GSFC who assist in evaluating the accuracy and utility of the data for their particular research applications. The information and experience gathered from experimentation with this initial instrument will be used in the development of an improved LAPR, currently in the design phase. This paper reports progress to date on the development, operation, and evaluation of the current instrument and notes areas of continuing research. See Blaine et. al., 1980, for engineering details of the LAPR.

The following discussion of pushbroom techniques is adapted from Thompson (1979). Pushbroom scanning is a term used to describe the technique of using the forward motion of an aircraft or satellite platform to sweep a linear array of detectors, oriented perpendicular to the ground track, across a scene being imaged. One array is typically used for each spectral channel. The platform motion provides one direction of scan, and electronic sampling of the detectors in the crosstrack dimension provides the orthogonal scan component to form an image. The detector array is sampled at the appropriate rate so that contiguous lines are produced.

Recent papers in the literature discuss the potential application of linear array technology to the remote sensing of earth resources. Thompson (1979) describes the advantages of using pushbroom scan techniques with linear arrays of solid state detectors as twofold: (1) complex

mechanical scan mechanisms are eliminated, allowing the precise geometric positioning of detectors; (2) the dwell time per resolution element is increased, resulting in an increased signal sensitivity and a significant improvement in the signal-to-noise ratio. A disadvantage is the manyfold increase in the number of detectors which must be calibrated. Tracy and Noll (1979) discuss the calibration procedures needed to radiometrically correct this data by compensating for variations in the detector responses caused by thermal drifts, dark current variations, and differences in electrical characteristics between detectors. Thompson (1979) presented evidence that such calibration is feasible and effective under laboratory conditions. The following sections discuss the LAPR design and components, the instrument's radiometric sensitivity, data preprocessing, and flight testing.

II. LAPR DESIGN AND COMPONENTS

Structural Design

The LAPR instrument consists of three major structural parts as shown in Figure 1: the three linear array sensors, the optical bench plate, and the sensor electronics unit. Each sensor (Figure 2) is essentially an independent narrow spectral band radiometer consisting of a linear array of photodiodes, thermo-electric coolers, lens, shutter, light baffle, and optical filter. The detectors are commercially available Reticon RL512C* linear arrays of silicon photodiodes. Each array contains 512 photodiodes manufactured on 25μm centers. The photosensitive area of each diode is 18μm x 25μm. Two thermo-electric coolers, placed on each side of an array, cool each detector to $1^{o}C \pm 1^{o}$. The cooling stabilizes and minimizes the detector dark current variations which are sensitive to the temperature of operation.

Each of the three radiometer units is sealed in a pressurized housing containing a dry nitrogen gas. Each unit consists of a near diffraction limited, ten element, Model 00385 Cine Nikkor CCTV lens, a light baffle, a remotely controlled shutter, an interference band pass filter, and the detector array. Filters may be interchanged by demounting the lens. For a description of the

*Trade names are given for description purposes only, and do not imply endorsement by NASA.

13 currently available filters, see Table 1. The shutter can be closed to block the incoming radiation thereby producing a black or zero signal for detector dark current calibration.

The three sensors are aligned on the optical bench plate, each using three point suspension to achieve coincident alignment of the sensors by boresighting. The alignment is necessary for the generation of multispectral data with the structurally independent sensors. The alignment assures that corresponding elements of the three arrays image nearly identical spatial views, with less than 10 pixels misregistration.

Optical Design

The optical design of the instrument was governed by the available detector array geometry, the practical radiometric requirements, and the decision to use commercially available lenses to minimize costs. The Nikon lenses that were finally chosen provide a 1.12 radian (64.2°) field of view (FOV) and maintained a near-diffraction limited performance for each detector over the entire array. At field angles greater than 0.56 radians (from nadir) the transmitted radiation is affected by lens vignetting. The 10mm nominal focal length of these lenses rendered the use of a single lens dichroic system impractical. Instead, the LAPR uses three separate optical units, with provision for boresighting and focusing. The lens can be adjusted from f/1.8 to f/10. The lens was set at f/4 for data acquisition to provide maximum irradiance without vignetting within the 64.2° FOV. The light transmission of the lenses is approximately 80 percent. The individual detectors have an instantaneous field of view (IFOV) of 0.146° or 2.54 milliradians which is well within the resolving (0.5 milliradians) power of the lens. The IFOV's of individual detectors do not overlap, thus the total field of view of the array is 1.3 radians (74.5°). Since the FOV of the lenses is 1.12 radians, the responses of approximately 36 detectors on either edge of the array are affected by lens vignetting. Due to this vignetting, only data from the 440 center detectors should be used for analysis.

An advantage of the LAPR is the capability to change optical filters between flights. The photodiodes of the three arrays are sensitive to radiation within the wavelength interval of 400

to 1000nm. (Figure 3), and the selectable integration time of the instrument allows the use of filters with narrow to wide bandwidths within this interval.

In the original configuration of the LAPR, the spectral filters were mounted in front of the lens (object space). Since the band pass filters are of the multi layered interference design, mounting them in front of the lenses results in a shift of the bandpass transmitted through the filters as the edge of the field of view is approached. Transmitted radiant energy from ±30° off the optic axis is blue shifted by approximately 40nm compared to the radiation transmitted on axis. Through an extensive laboratory bench study of the lens' optical characteristics it was found that by mounting the filter between the lens and detectors (image space) that this angular variation could be reduced. This makes the blue shift negligible (~2nm) when compared to the filter bandpass of (45nm) measured at Full Width at Half Maximum (FWHM). This method of filter attachment is now used.

Electronic Design

The LAPR electronics operate the linear arrays in an integrating mode and provide signal processing circuitry and clocking and scanning logic which control the sampling of data from the arrays. Both quantized video signals from the arrays and housekeeping information for radiometric correction and system validation are recorded during LAPR operation. Unlike the detectors of conventional mechanical scan mechanisms, the LAPR photodiodes sense radiant flux integrated over a period of time. For example, the dwell time per resolution element in the Landsat Multispectral Scanner (MSS) is 14 microseconds. Using a pushbroom approach under the same orbital conditions, the dwell time can be increased to 12 milliseconds for the same resolution dimension (Thompson, 1979). A photodiode exhibits internal capacitance, and hence will hold an electric charge. Subsequent photoconduction reduces the charge at a rate proportional to the incident radiant flux. For the array technology used in this sensor, the charge required to recharge a photodiode to a reference voltage is proportional to the integral to incident radiant flux over the period between charges; i.e., the integration time (Castleman, 1979). The digital value recorded for each detector during operation is proportional to the recharge current.

is

o

s

ie

array scan interval can be set from 66 ... craft

altitude and speed for a given mission to insure that contiguous scans of the terrain are ned. The clocking pulses and sating circuitry enable the sequential readout of the video signals from the 512 individual diodes of an array, eliminating the need for a separate connection for each detector.

The video signals from the three arrays are read out simultaneously, clocked through buffer-amplifiers and multiplexers, and quantized from an analog signal to an eight bit digital word (byte). The data is then sent to the digital multiplexor, formatted into 1551 byte records, and then sent to a tape recorder and system moniter. Each scan line is stored as a single record consisting of the data from each of the three arrays and the housekeeping information. The date and time of the flight, the integration and scan time, a 6.2 volt reference voltage, 6 sensor temperature readings, and a roll angle signal are recorded as housekeeping data. The temperature measurements are obtained from two thermistor sensors located in each of the sensor assemblies. The data are used to monitor any temperature changes in the sensors which may cause thermal drifts in the data. The roll angle signal is generated from a Lear Siegler Model 9000J vertical gyroscope mounted on the instrument. The roll signal is used in a data preprocessing step to correct geometric image distortion due to aircraft roll.

The system monitor circuitry checks the position and value of the reference voltage byte in the 1551 byte record to determine if the electronics system is functioning properly. The digital tape recorder, a Kennedy Model 9000, records data on 800 bpi, 9-track magnetic tape. With a

scan interval of 150ms, a 2400 ft. data tape will last approximately 20 minutes. Tapes can be changed during a flight, but continuous flight lines are limited to the 20 minute tape duration.

Aircraft Interface

The instrument was attached to the forward right side of the cabin floor of a Twin Beech C-45 aircraft. The tape recorded, LAPR control panel, buffer/amplifier, and time code generator were fastened to a specially constructed rack attached to the side of the aircraft cabin. A nine by nine inch format aerial camera was also attached to collect either coincident color, color infrared, or black and white photography during data runs. As an aid to flight path alignment, a downward pointing television camera was installed with monitors in the cockpit and cabin.

III. RADIOMETRIC SENSITIVITY

The radiometric sensitivity of an individual detector can be expressed in terms of noise equivalent reflectivity (NErho). The noise equivalent reflectivity is the percent change in target reflectivity equivalent to the root mean squared (rms) noise of a detector (Thompson, 1979). In other words, the reflectivities from two targets must differ by at least NErho before the change in detector response can be distinguished from the inherant noise of the sensor system. NErho is a function of detector noise, sensor optical throughput characteristics, filter bandpasses, detector integration time, atmospheric conditions and sensor altitude, target irradiance, and target reflectivity.

In order to quantitatively assess the NErho for LAPR detectors, the various factors affecting sensitivity must be evaluated. First, detector noise can be described by the noise equivalent signal (NES). NES is the detector root mean squared (RMS) noise in units equivalent to exposure density at the focal plane ($\mu J/m^2$). This measure of detector sensitivity is derived from the fact that the detectors operate in an integrating mode. NES is obtained by exposing a detector to a known radiance level and measuring the signal to noise ratio. Optical parameters allow the conversion from radiance to irrandiance at the detector, and the irradiance is then multiplied by the

integration time. NES is equal to this exposure density divided by the signal to noise ratio:

$$NES = \frac{\pi N_{\Delta\lambda} \tau_o t}{4(f/\#)^2 (S/N)}$$

where

$N_{\Delta\lambda}$ = Spectral radiance for a bandpass of $\Delta\lambda$

τ_o = Optical transmission (throughput)

t = integration time

$f/\#$ = f stop sitting of the lens

S/N = signal to noise ratio

The NES of the nadir detector (256th detector) was selected for the NErho calculations.

Next, optical throughput parameters are considered. The product of the lens transmission (0.80) and the filter transmission (0.75) gives an optical transmission of 0.6 for each LAPR sensor at the near nadir detectors. The transmission of the lenses for off axis incident radiation, however, is proportional to the fourth power of the cosine of the incident field angle ($\cos^4 \theta$). Thus, transmission at the extreme angles of incidence (±30°) is approximately half that for radiation parallel to the optical axis (cos 30° = 0.5625), and the NErho's for the detectors at the ends of the array are approximately double the NErho's for the near nadir detectors.

Having considered detector noise and optical throughput, Table 2 presents an assessment of LAPR radiometric sensitivity based on radiances derived from an atmospheric model provided by Fraser (1975) for typical target spectral reflectivities. The following conditions are assumed: sensor altitude of 12km; a solar zenith angle of 50° (typical for midday in the U.S. during Spring); and a clear atmosphere over a rural area with 27km visibility. As previously emphasized, NErho varies across a detector array due to variation in RMS noise from detector to detector and the reduction of lens transmission with off axis field angles. Still, the NErho's of the center detectors are small and compare favorably to the sensitivity of the Thematic Mapper (TM) planned for

Landsat-D or the Multispectral Scanner (MSS) systems of the first three Landsat satellites (Table 3).

IV. DATA PREPROCESSING

Radiometric Correction

The raw digital data generated by LAPR are radiometrically corrected as a ground preprocessing step to compensate for dark current and response variations from detector to detector. The raw digital value from the ith detector, Vi, is transformed to a corrected value, VCi, using the following first order formula:

$$VCi = (Vi - Oi)(Gi),$$

where Oi is the detector offset or dark current reference, and Gi is the gain correction factor. This approach assumes a strictly linear detector response. The dark current reference, Oi, is recorded in flight for each detector by closing the shutter for several scan intervals immediately preceeding and following data acquisition.

The gain correction factor, Gi, is derived from a laboratory multi radiance level calibration. For calibration, each sensor/filter combination is positioned to view an opening in a six foot diameter integrating sphere. The response of each of the 512 detectors is recorded for each calibrated level of sphere radiance. Approximately 200 sequential data points are recorded from each detector at each radiance level to permit a mean response and a response variance to be calculated for each detector. A least squares regression line expressing response as a linear function of radiance is then computed for each detector. The gain correction factor, Gi, is given by the following formula:

$$Gi = A256/Ai,$$

where Ai is the slope of the regression line for the ith detector and A256 is the slope for the nadir detector. In principle, this assures that the corrected values are consistant across the array for a uniform and constant radiance level across the instrument's field of view. The nadir element serves as a reference since lens transmission is maximum at nadir.

Evaluation of Radiometric Correction

A laboratory experiment was performed to verify the effectiveness of the correction techniques described above. The experiment involved having each filter/sensor combination view the integrating sphere at several radiance levels as before. Assuming the radiance from the integrating sphere was uniform across the sensor field of view, a plot of corrected detector response versus detector array position should result in a horizontal line.

Such plots, however, showed considerable response fluctuations across an array, and the range of corrected response values amounted to 10 to 15 percent of the mean response at a constant radiance level (i.e., a response range of 105–115 with a mean response of approximately 110 in Figure 4). The spread of response values about the mean response tended to increase with the magnitude of the radiance levels. Figure 4 shows a plot of corrected response (ordinate) versus detector number (abscissa) for a spectral radiance level of 7.09μW/Ster-cm^2 -nm and a filter with 462 to 507nm bandpass.

To improve our understanding of radiometric correction, several aspects of the current procedure require further investigation. First, the uniformity of the reflecting surface in the integrating sphere will be assessed. Each detector in an array views only a small portion of the sphere's interior surface, and reflectivity variations across the surface will adversely affect the instrument calibration. The linearity of detector response will also be evaluated, and departures from linearity will be quantified. These investigations will lead to improved correction procedures perhaps based on expressing detector response as a polynomial or piecewise linear function of radiance.

Geometric Correction

The roll angle of the LAPR in flight is measured by a vertical gyro mounted on the instrument and a digital measurement of roll is recorded with each scan line. The roll is compensated by shifting the pixels in the scan line by an amount proportional to the roll angle using the following equation: PSA = 6.6871 (RA), where PS is the pixel shift and RA is the roll angle. The roll angle was nominally ±3 degrees for data acquisition flights during 1979.

Other geometric distortions of LAPR digital data are not routinely corrected during data preprocessing. Distortions due to pitch and yaw of the platform aircraft did not hamper the interpretation of the test imagery and were not corrected. A scan angle, or foreshortening, distortion also occurs in LAPR imagery because the ground IFOV's of the detectors increase with distance from the center of the array (the IFOV of extreme detectors is 1.33 times the IFOV of the center detector). This foreshortening distortion is common to most airborne electrooptical scanners. Algorithms for correcting this distortion are provided by numerous image processing systems. Image distortion caused by errors in matching the scanning rate of the LAPR to the aircraft ground speed creates scan overlap or underlap, which are not corrected. However, such distortions were not visually evident in any LAPR data collected to date.

Data Tape Format

The end product of data preprocessing is a 9 track computer compatible tape (CCT) for the LAPR data user. The CCT contains the radiometrically and geometrically corrected LAPR data at a density of 800 bits per inch (bpi) written with odd parity in a band sequential format (i.e., one file per data channel). Each record of a data file represents one scan line and consists of 512 eight-bit bytes. Each byte is the response from a single LAPR detector. The CCT contains no file or record header information.

V. FLIGHT TEST PROGRAM - 1979

To evaluate the potential application of LAPR data, the instrument was flown on a trial basis in support of ongoing research conducted by the Earth Resources Branch at NASA/GSFC. The research projects included: mapping forest canopy gypsy moth defoliation in Central Pennsylvania; monitering strip mine reclamation in Northeastern Pennsylvania; and mapping urban land cover between Baltimore, Maryland, and Washington, D.C. Table 4 lists characteristics for flights over each test area. Prior to evaluation, the LAPR data had been roll and radiometrically corrected. Data from the entire array was used for evaluation. False composite images, black and white images for each channel, and thematic maps were derived from selected subsets of the test flight imagery, using the General Electric Image 100 interactive digital analysis system at GSFC.

The false color images were displayed on the Image 100 cathode ray tube (CRT) for examination. The data from channels one, two, and three were displayed as red, green, and blue, respectively to simulate color infrared photography. A consistant misregistration between channels was apparent in all images. Channels 1 and 2 appeared to be registered, but channel 3 was misaligned in one dimension, parallel to the scan line. The misalignment was corrected using Image 100 software, by laterally shifting the Channel 3 image 8 pixels to the right. After shifting, the channels appeared to be registered within one pixel of each other.

Following channel registration, the roll correction was visually evaluated. Examination of linear features such as highways or railroads parallel to the flight line revealed that the distortion due to roll had been reduced to an acceptable level. On this basis the roll correction was judged to be effective.

A detailed visual inspection of the black and white imagery of the separate channels revealed a slight vertical (parallel to the flight line) striping in channels 2 and 3 for the Laurel and Marysville scenes. The striping was most apparent over areas with low reflectivity in these bands (i.e., forest vegetation) especially near the edges of the image. The observed vertical banding was attributed to the increased visual impact of system noise and calibration error at low signals. The system noise is assumed to have a fixed distribution over the entire array. The visual impression of striping is most noticeable in areas with low reflectivity since the noise would constitute a greater percentage of the signal. In other words, a difference of five or six gray levels due to noise between neighboring detectors would be more apparent in areas with a mean signal of 30, than in areas with a mean signal of 180. System noise is compounded at the edge of the images by the radiometric correction procedures. The magnitude of the gain correction factor is larger for detectors at the edges of the arrays to compensate for the decreased transmittance of the lens at the edges of the FOV. This conclusion is supported by the observation, in the test imagery, that areas with higher reflectivity such as bare soil, roof tops, concrete or asphalt paving in channels 2 and 3, or vegetation in channel 1, did not show any visible signs of vertical banding, even for the extreme off nadir detectors.

A slight horizontal banding was also detected in the test images. This was attributed to periodic noise in the power source aboard the platform aircraft and not the LAPR instrument itself. The power source problem has been corrected and should not affect data acquired in the future.

A subset of the LAPR data for near infrared (channel 1) of the Laurel, MD image is shown in Figure 5. The image was subset to eliminate the wavy edges caused by roll correction. The Laurel image contains the greatest diversity of cover types among the test sites. Channel 1 shows the greatest amount of detail among the three bands.

A preliminary digital analysis of the LAPR test imagery was conducted on the GE Image 100 system. This analysis consisted of mapping the relevant land use categories for each study using a parallelpiped classifier. The category statistics used to train the classifier were generated by supervised trained on sites representing land cover categories of interest, as identified by visual comparison with aerial color infrared photography taken during the LAPR overflights. The urban test area near Laurel, in Prince Georges County, MD included hardwood forest, open fields, exposed soil, commercial/industrial tracts, multi and single unit dwellings, and recreational areas. The forest test area near Marysville, in Perry County, PA., included a hardwood forest with severe tree mortality resulting from heavy gypsy moth defoliation in 1977, healthy hardwood forest, agricultural land, single unit dwellings, and commercial areas. The strip mine study in Clarion County, PA., included active strip mines, areas in various stages of reclaimation, hardwood forests, and agricultural land. Table 5 lists the land cover categories identified for each image. Visual comparison of the thematic maps derived from the LAPR data with the aerial photography indicated an accurate mapping of the land cover categories.

VI. CONCLUSIONS

The functional characteristics of an experimental Linear Array Pushbroom Radiometer (LAPR) have been described. The radiometric sensitivity of the LAPR was defined in terms of its noise

equivalent reflectivity (NErho), and was favorably compared with the NErho's for the Landsat MSS and the Thematic Mapper. The data preprocessing steps, including radiometric correction and roll correction were described. The radiometric correction was evaluated quantitatively under laboratory conditions and qualitatively in the first testing program. The flight tests were much better than could be predicted by the laboratory evaluation.

Imagery derived from LAPR test flight data were found to have slight vertical banding over relatively low reflective areas at the edges of the detector array. This was attributed to the increased impact of system noise upon low throughput signals, compounded by the larger gain correction factors used for the near edge detectors. Alternative methods for improved radiometric calibration and radiometric correction are being developed. Other anomalies in the LAPR data were found to be easily corrected, or not related to the LAPR instrument itself. Although effective radiometric correction could not yet be demonstrated via laboratory testing, radiometric distortion did not preclude the visual interpretation or parallelpiped classification of the three test areas.

Such encouraging results from the first experimental LAPR instrument developed by NASA clearly indicates the promise of MLA technology to remote sensing, particularly since improved linear array instruments and radiometric calibration procedures are currently being developed from the experience gained from the collection and analysis of data from the first LAPR.

VII. ACKNOWLEDGMENTS

The authors wish to acknowledge the technical support and contributions to this paper by the following members of the Earth Observations Systems Division: Chuck Mason, Fred Blaine, Bob Sullivan, Ken Brown, and Les Thompson. The authors also recognize the aircraft support provided by NASA/Wallops Flight Center.

VIII. REFERENCES

1. Blaine, L. R., K. S. Brown, M. W. Finkel, F. G. Huegel, C. C. Mason, and R. J. Sullivan, 1980. "The Construction and Calibration of a Solid State Linear Array Pushbroom Radiometer," (in preparation).

2. Castleman, K. R., 1979. Digital Image Processing. Prentice-Hall, Inc., Englewood Cliffs, NJ.

3. Fraser, R. S., 1975. "Radiances for Thematic Mapper," Memorandum from R. S. Fraser to Distribution, July.

4. Thompson, L. L., 1979. "Remote Sensing Using Solid-State Array Technology," Photogrammetric Engineering and Remote Sensing, Vol. XLV, No. 1, pp. 47-55.

5. Tracy, R. A., and R. E. Noll, 1979. "User-Oriented Data Processing Considerations in Linear Array Applications," Photogrammetric Engineering and Remote Sensing, Vol. XLV, No. 1, pp. 57-61.

Table 1
Description of the Spectral Band Pass Filters Available for the LAPR Instrument

Number	Bandpass (nm) FWHM*	λ_0 (nm)	$\Delta\lambda$ (nm)	Filter Diameter (in)	Percent Transmittance	TM Band
1	462.5 -507.5	485.0	45.0	2	0.62	
2	459.0 -528.2	493.6	69.2	2	0.61	1
3	540.5 -558.5	549.5	18.0	1	0.60	
4	509.0 -599.8	574.4	90.8	2	0.60	2
5	537.5 -582.5	560.0	45.0	2	0.62	
6	577.5 -622.5	600.0	45.0	2	0.64	
7	627.8 -677.7	652.8	49.9	2	0.54	3
8	633.2 -672.2	669.7	13.0	1	0.68	
9	729.7 -744.1	736.9	14.4	1	0.53	
10	738.25-755.75	747.0	17.5	1	0.63	
11	780.55-793.05	786.8	12.5	1	0.61	
12	759.0 -882.4	820.8	123.4	2	0.62	4
13	802.5 -847.5	825.0	45.0	2	0.58	

*FWHM - Full Width at Half Maximum

Table 2

LAPR Radiometric Sensitivity Measurements for the Four Array/Filter Combinations Used in the 1979 Flight Test Program

Detector Array Designation	Filter λ_o (micrometers)	Filter $\Delta\lambda$ (micrometers)	NES for Center Detector ($\mu J/m^2$)	Total Sensor Radiance $N^{\tau}_{\Delta\lambda}$ (w/m^2-st)	Path Sensor Radiance $N^{\rho}_{\Delta\lambda}$ (w/m^2-st)	Noise Equivalent Reflectance-Center Detector $NE\Delta\rho$ in Percent
1	0.485	0.045	18	3.86	1.57	0.23%
2	0.560	0.045	22	7.22	1.49	0.28%
2	0.600	0.045	25	6.36	0.95	0.33%
3	0.825	0.045	36	6.71	0.80	0.65%

Table 3
Radiometric Sensitivity Statistics for the Spectral Bands Used in the Thematic Mapper and Multispectral Scanner

	Thematic Mapper (TM)		Multispectral Scanner Subsystem (MSS)	
	Micrometers	Radiometric Sensitivity (NE$\Delta\rho$)	Micrometers	Radiometric Sensitivity (NE$\Delta\rho$)
Spectral Band 1	0.45 0.52	0.8%	0.5 0.6	0.57%
Spectral Band 2	0.52 0.60	0.5%	0.6 0.7	0.57%
Spectral Band 3	0.63 0.69	0.5%	0.7 0.8	0.65%
Spectral Band 4	0.76 0.90	0.5%	0.8 1.1	0.70%
Spectral Band 5	1.55 1.75	1.0%		
Spectral Band 6	2.08 2.35	2.4%		
Spectral Band 7	10.40 12.50	0.5K (NEΔT)		

Table 4
LAPR Flight Characteristics

Project	Study Area Location	Flight Date	Local Flight Time	Altitude (meters-above mean-datum)	Resolution at Nadir (m)	Filter Spectral Bandwidths (nm)		
						Array 1	Array 2	Array 3
Surface Mine Reclamation	Clarion County, Pennsylvania	5/17/79	1200	3000	7.5	802.5–847.5	577.5–622.5	462.5–507.5
Urban Land Cover	Laurel, Prince Georges' County, MD	8/17/79	1200	2900	7.2	802.5–847.5	577.5–622.5	537.5–582.5
Forest Defoliation	Marysville, Perry County, PA	6/27/79	1130	3000	7.5	802.5–847.5	577.5–622.5	462.5–507.5

Table 5
Land Cover Categories as Derived from LAPR Test Flight Data

Forest Defoliation	Surface Mine Reclamation	Urban Land Cover
Water (River)	Forest	Forest
Lawns & Open Fields	Agricultural & Open Fields	Lawns & Open Fields
Open Canopy Forest	Revegetated Mine Spoil (forbes and Legumes)	Asphalt Paving
Closed Canopy Forest	Bare Soil and Mine Spoil	Bare Soil (construction)
Rooftops & Concrete Paving	Coal Refuse	Water (small ponds)
Railroad Yard & Asphalt Paving		Residential Streets & Single Unit Dwellings
Shaded Vegetation (under Open Canopy)		Industrial Buildings

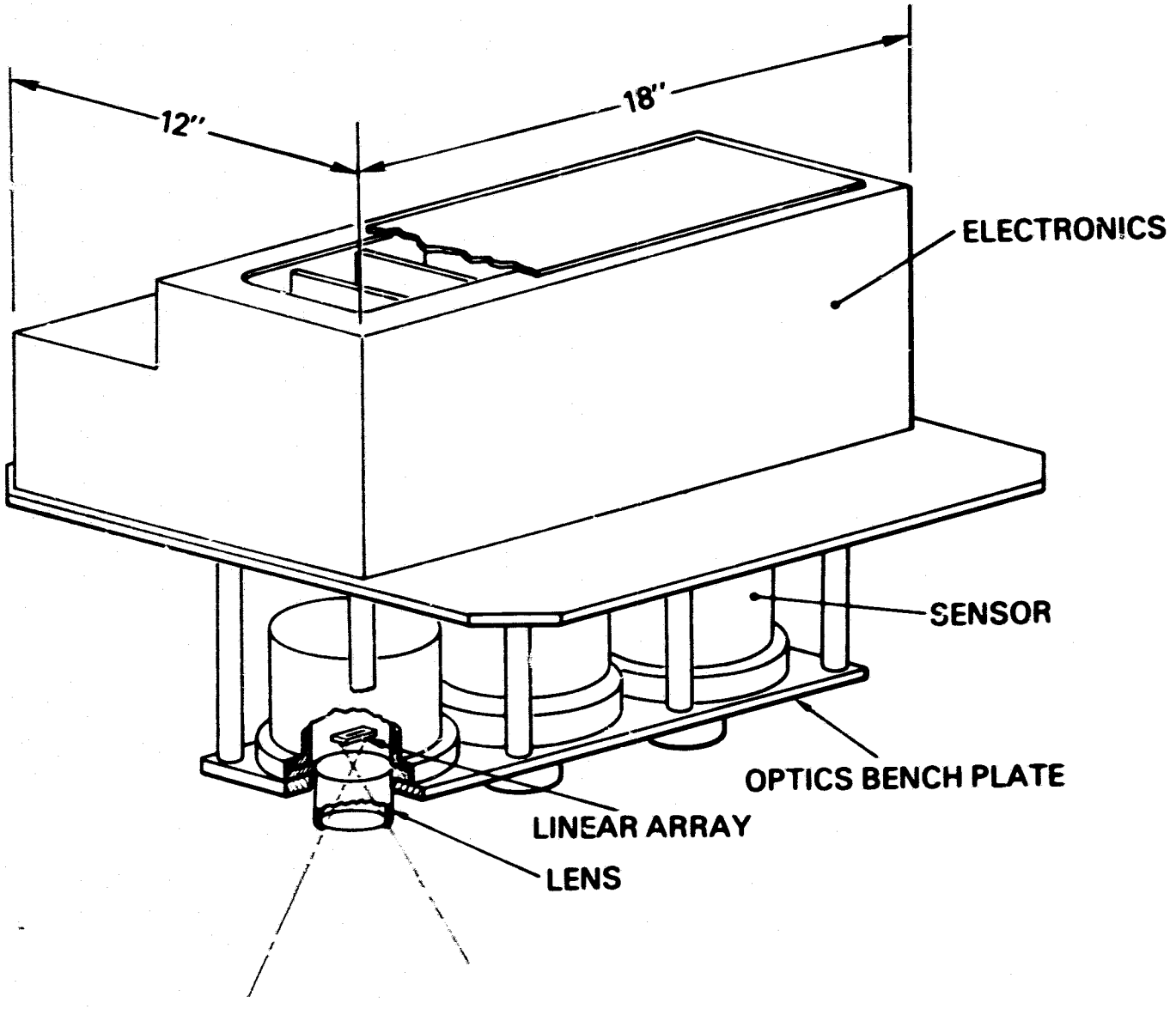

Figure 1. Structural Components of the LAPR Instrument

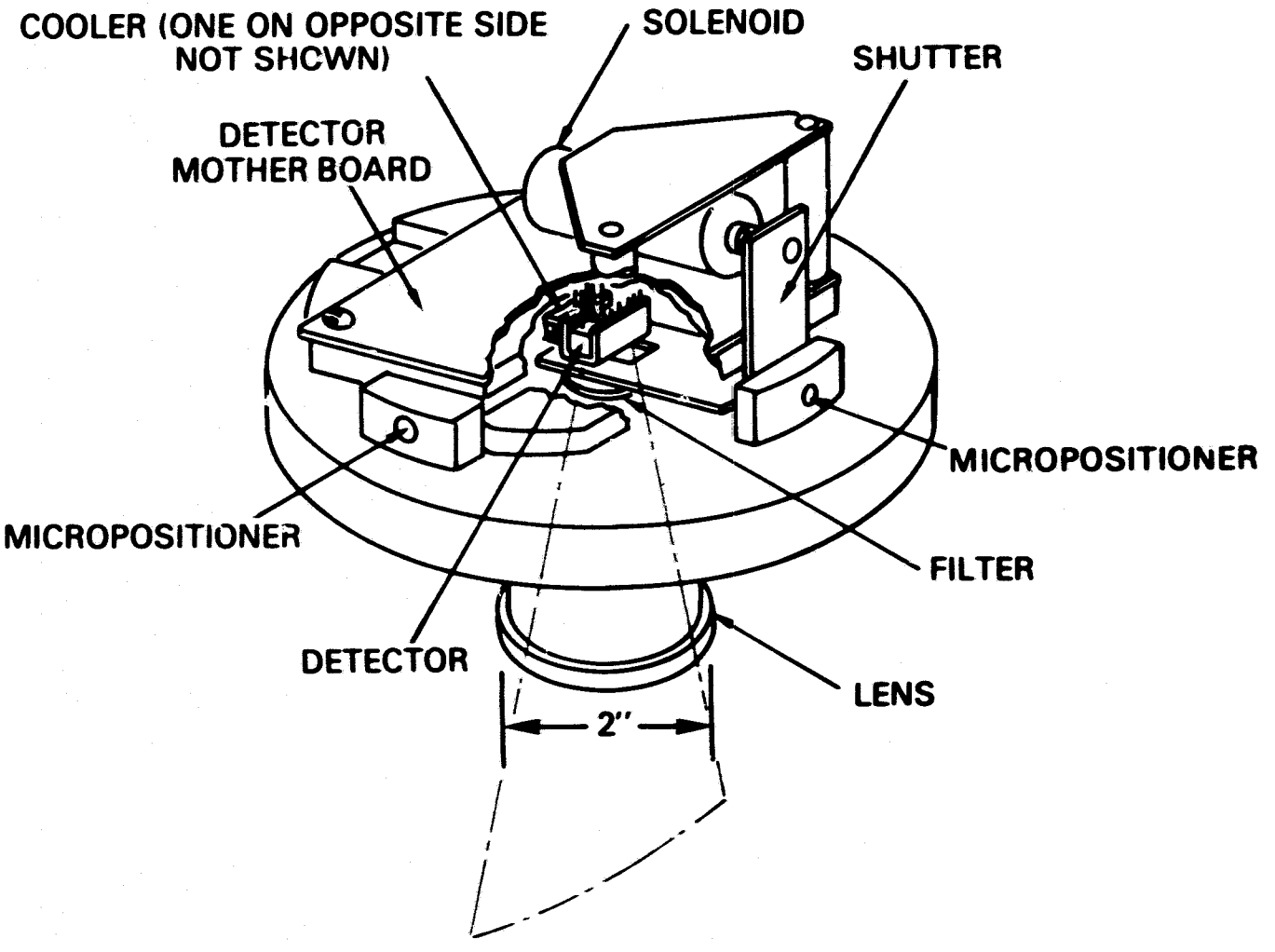

Figure 2. Diagram of a LAPR Sensor

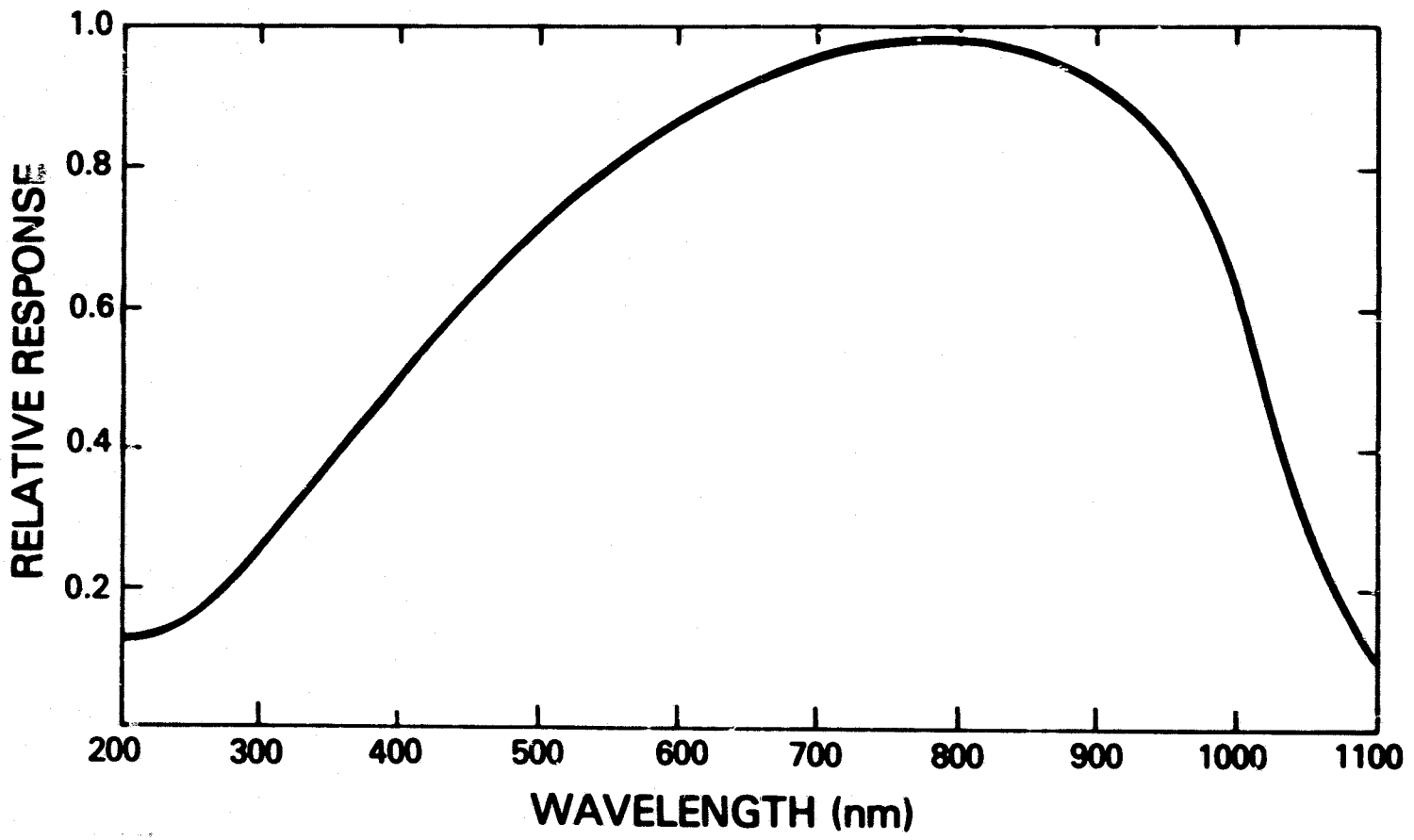

Figure 3. Response Curve of a Typical Detector Element Between 200 and 1100nm

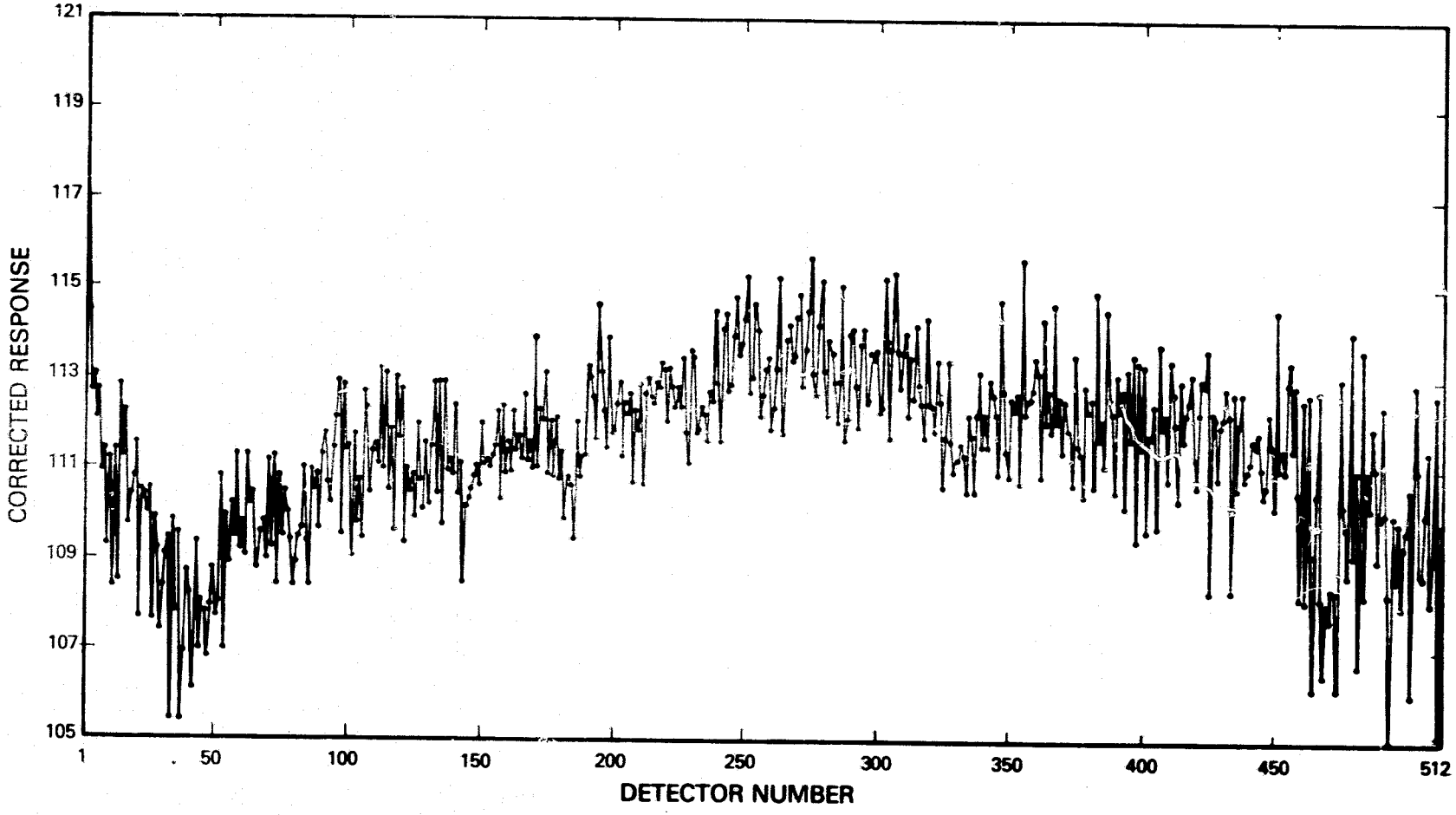

Figure 4. Plot of the Corrected Response Vs. Detector Number for a Spectral Radiance Level of 7.09μW/Ster/cm^2/nm

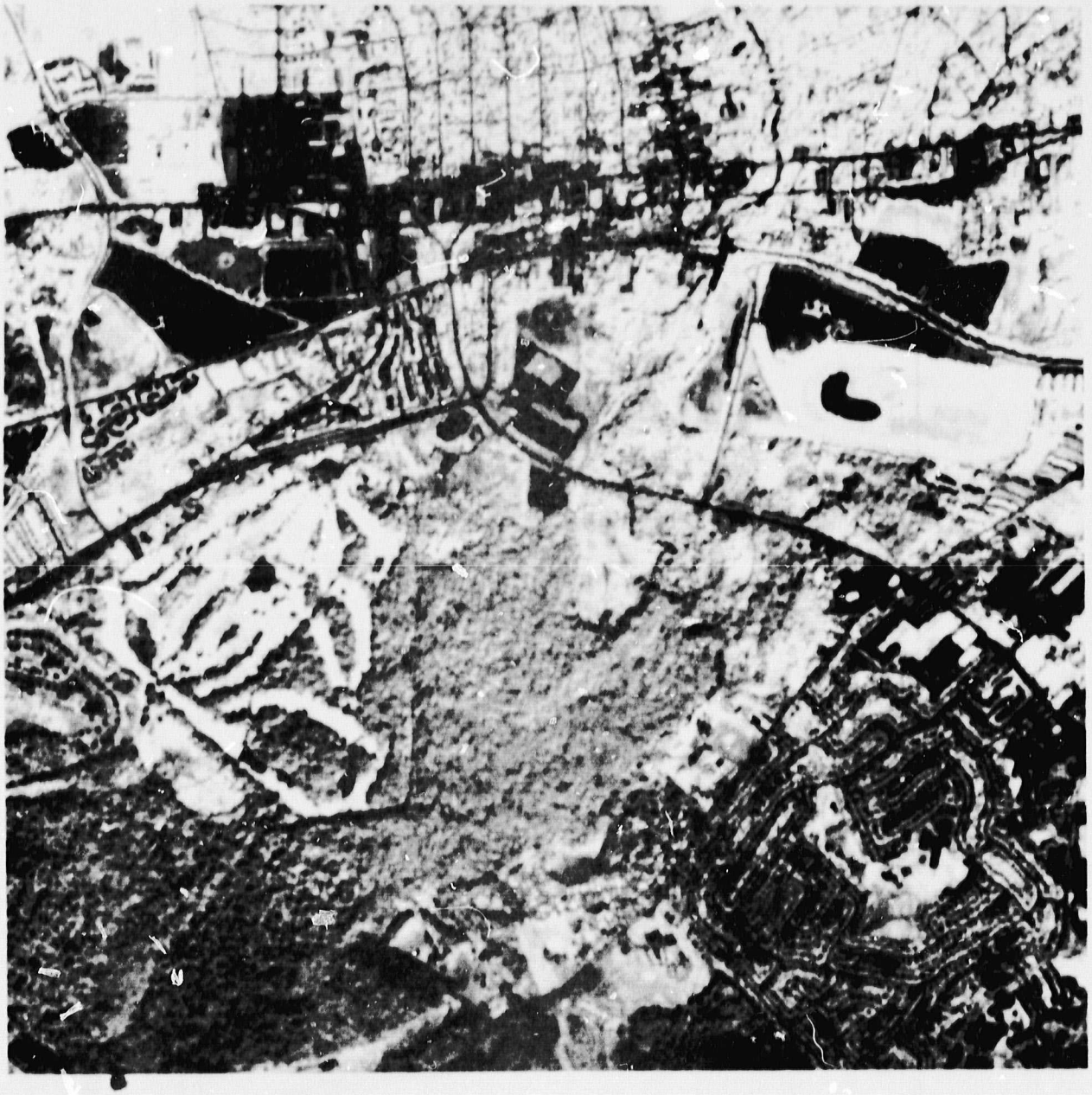

Figure 5. Channel 1, Near-Infrared (802.5 - 847.5 nm) LAPR Image Collected over Laurel, MD

FIGURE CAPTIONS

Figure 1. Structural Components of the LAPR Instrument

Figure 2. Diagram of a LAPR Sensor

Figure 3. Response Curve of a Typical Detector Element Between 200 and 1100nm

Figure 4. Plot of the Corrected Response Vs. Detector Number for a Spectral Radiance Level of 7.09μW/Ster/cm^2/nm.

Figure 5. Channel 1, Near-Infrared (802.5 - 847.5nm) LAPR Image Collected over Laurel, MD